A&A 603, L1 (2017)
DOI: 10.1051/0004-6361/201731121

Astronomy & Astrophysics

Letter to the Editor

NH_3 (1_0–0_0) in the pre-stellar core L1544*

P. Caselli[1,2], L. Bizzocchi[1], E. Keto[3], O. Sipilä[1], M. Tafalla[4], L. Pagani[5], L. E. Kristensen[6], F. F. S. van der Tak[7,8], C. M. Walmsley[2,9,y], C. Codella[2], B. Nisini[10], Y. Aikawa[11], A. Faure[12], and E. F. van Dishoeck[13,1]

[1] Centre for Astrochemical Studies, Max-Planck-Institute for Extraterrestrial Physics, Giessenbachstrasse 1, 85748 Garching, Germany
e-mail: caselli@mpe.mpg.de
[2] INAF–Osservatorio Astrofisico di Arcetri, Largo E. Fermi 5, 50125 Firenze, Italy
[3] Harvard-Smithsonian Center for Astrophysics, 60 Garden Street, Cambridge, MA 02138, USA
[4] Observatorio Astronómico Nacional (IGN), Calle Alfonso XII, 3 Madrid, Spain
[5] LERMA and UMR 8112 du CNRS, Observatoire de Paris, 61 Av. de l'Observatoire, 75014 Paris, France
[6] Centre for Star and Planet Formation, Niels Bohr Institute and Natural History Museum of Denmark, University of Copenhagen, Øster Voldgade 5–7, 1350 Copenhagen, Denmark
[7] SRON Netherlands Institute for Space Research, Landleven 12, 9747 AD Groningen, The Netherlands
[8] Kapteyn Astronomical Institute, University of Groningen, The Netherlands
[9] The Dublin Institute for Advanced Studies, 31 Fitzwilliam Place, Dublin 2, Ireland
[10] INAF–Osservatorio Astronomico di Roma, 00040 Monte Porzio Catone, Italy
[11] Center for Computational Science, University of Tsukuba, Tsukuba, 305-8577 Ibaraki, Japan
[12] Université Grenoble Alpes, CNRS, IPAG, 38000 Grenoble, France
[13] Leiden Observatory, Leiden University, PO Box 9513, 2300 RA Leiden, The Netherlands

Received 7 May 2017 / Accepted 8 June 2017

ABSTRACT

Pre-stellar cores represent the initial conditions in the process of star and planet formation, therefore it is important to study their physical and chemical structure. Because of their volatility, nitrogen-bearing molecules are key to study the dense and cold gas present in pre-stellar cores. The NH_3 rotational transition detected with *Herschel*-HIFI provides a unique combination of sensitivity and spectral resolution to further investigate physical and chemical processes in pre-stellar cores. Here we present the velocity-resolved *Herschel*-HIFI observations of the ortho-NH_3(1_0 0_0) line at 572 GHz and study the abundance profile of ammonia across the pre-stellar core L1544 to test current theories of its physical and chemical structure. Recently calculated collisional coefficients have been included in our non-LTE radiative transfer code to reproduce *Herschel* observations. A gas-grain chemical model, including spin-state chemistry and applied to the (static) physical structure of L1544 is also used to infer the abundance profile of ortho-NH_3. The hyperfine structure of ortho-NH_3(1_0 0_0) is resolved for the first time in space. All the hyperfine components are strongly self-absorbed. The profile can be reproduced if the core is contracting in quasi-equilibrium, consistent with previous work, and if the NH_3 abundance is slightly rising toward the core centre, as deduced from previous interferometric observations of para-NH_3(1, 1). The chemical model overestimates the NH_3 abundance at radii between ' 4000 and 15 000 AU by about two orders of magnitude and underestimates the abundance toward the core centre by more than one order of magnitude. Our observations show that chemical models applied to static clouds have problems in reproducing NH_3 observations.

Key words. astrochemistry – line: profiles – radiative transfer – methods: observational – ISM: clouds – ISM: molecules

1. Introduction

Since its discovery as the first polyatomic molecule in space (Cheung et al. 1968), ammonia has been widely used as a temperature and structural probe of dense cloud cores in low-mass (e.g. Benson & Myers 1989) and high-mass (e.g. Pillai et al. 2006) star-forming regions, and as a tracer of shocks along outflows driven by young stellar objects (e.g. Tafalla & Bachiller 1995). NH_3 can form on the surface of dust grains through hydrogenation of atomic nitrogen and in the gas phase soon after the formation of N_2. Unlike molecules such as CO, NH_3 does not appear to be affected by freeze-out within dense and cold starless cores (Tafalla et al. 2002), despite its high binding energies (close to those of H_2O). While the inversion transitions of ortho (o) and para (p) NH_3 around 1.3 cm are easily accessible from the ground, the rotational transitions fall into the sub-millimeter and far-IR, and these can only be detected using space-borne receivers. The Einstein coefficients of the rotational transitions of NH_3 are about 10 000 times larger than those of the inversion transitions (Ho & Townes 1983), implying significantly higher critical densities (' 10^7 cm ^{3} vs. ' 10^3 cm ^{3}; Danby et al. 1988).

The first observation of the ground-state rotational transition of o-NH_3(1_0 0_0) was carried out by Keene et al. (1983) toward OMC-1 using the *Kuiper* Airborne Observatory (KAO). About twenty years 0(lio-359a6e)-511(f 68.171 -145 Td [((1,)-

* Based on observations carried out with *Herschel*, an ESA space observatory with science instruments provided by a European-led Principal Investigator consortium and with important participation from NASA.
y Deceased.

high-mass star-forming regions (Hjalmarson et al. 2005; Persson et al. 2007, 2009) and, for the first time, toward a dark cloud (ρ Oph A; Liseau et al. 2003). Multiple rotational transitions have also been detected using the Heterodyne Instrument for the Far Infrared (HIFI; de Graauw et al. 2010) instrument on board the *Herschel* Space Observatory in the direction of high-mass star forming regions (Persson et al. 2010; Gerin et al. 2016) and with the Infrared Space Observatory (ISO; Ceccarelli et al. 2002). The o-NH_3(1_0 0_0) has also been detected with *Herschel* by Codella et al. (2010) toward the shock region L1157-B1, by Salinas et al. (2016) toward the protoplanetary disk TW Hydrae, and by Lis et al. (2016) in the direction of the starless core L1689N, next to the young protostar IRAS16293-2422. None of the above spectra show resolved hyperfine structure of o-NH_3, including the one toward L1689N, where only one group of hyperfine components is detected. The 3_2 2_2 rotational transition of NH_3 at 1.8 THz has also been observed with the Stratospheric Observatory For Infrared Astronomy (SOFIA) by Wyrowski et al. (2012, 2016) to measure the infall rate in high-mass star-forming clumps.

We report the first detection of the hyperfine structure of o-NH_3(1_0 0_0) toward the isolated pre-stellar core L1544 in the Taurus molecular cloud complex, as part of the Water In Star-forming regions with *Herschel* (WISH) key project (van Dishoeck et al. 2011). The turbulence in L1544 is subsonic and the narrow spectral line widths, together with the high spectral resolution of HIFI, allow us to distinguish the quadrupole hyperfine structure that is due to the interaction between the molecular electric field gradient and the electric quadrupole moment of the nitrogen nucleus. These observations also confirm the dynamical structure that has been deduced by previous theoretical studies (Keto & Caselli 2008, 2010; Keto et al. 2015) constrained by ground-based (Caselli et al. 1999, 2002) and *Herschel* (Caselli et al. 2010, 2012) observations. In the following, we refer to the core envelope as the region beyond ' 4000 AU, where the number density drops below 10^5 cm ^{3} (Keto & Caselli 2010). Observations are described in Sect. 2, the o-NH_3(1_0 0_0) spectrum is shown in Sect. 3 and the analysis is presented in Sect. 4. Discussion and conclusions can be found in Sect. 5.

2. Observations

The o-NH_3(1_0 0_0) line (central frequency 572.49815977 GHz 0.2 kHz; Cazzoli et al. 2009) has been observed with *Herschel* toward the pre-stellar core L1544 (coordinates RA(J2000) = $05^h04^m17\overset{s}{.}21$, Dec(J2000) = 25 $10^0 42\overset{00}{.}8$) for 10.3 h on April 2, 2011, together with the o-H_2O(1_{10} 1_{01}) (Caselli et al. 2012). The data presented here are archived at the *Herschel* science archive[1] with the identification number (OBSID) 1342217688. The technical details of the observations, which include the simultaneous use of the wide-band (WBS) and the high-resolution (HRS) spectrometers of HIFI in both *H* and *V* polarisation, have been described in Caselli et al. (2012). We briefly summarise the details related to the HRS data for o-NH_3, which are used here: the half-power beam width (HPBW) of the telescope at 572 GHz is 40^{00} and the spectral (nominal) resolution is 64 m s ^{1} at 572.5 GHz. The individual spectra were reduced using the *Herschel* interactive processing environment (HIPE; Ott 2010), version 14.1, and subsequent analysis of the data was performed with the Continuum and Line-Analysis Single dish Software (CLASS) within the GILDAS package[2]. The latest in-flight-measured beam efficiencies were used to convert the intensity scale from antenna temperature into main-beam temperature (T_{mb})[3]. The H and V polarisation spectra are identical and they have been summed together to increase the sensitivity.

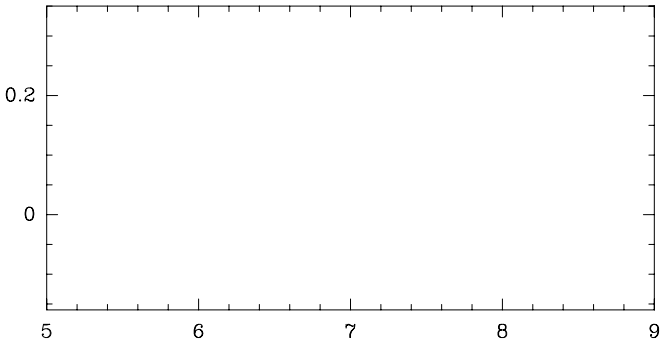

Fig. 1. *Herschel* HIFI spectrum of o-NH_3(1_0 0_0) toward the pre-stellar core L1544. The three groups of hyperfine components (with the 0 1 group having one single component) are detected for the first time in space. They are all highly self-absorbed (see Sect. 3). The hyperfine structure is shown by black vertical lines (with LTE relative intensities) and labelled as in Cazzoli et al. (2009). The vertical dotted line marks the core velocity. The root-mean-square noise level is 4.7 mK.

3. Results

The continuum-subtracted o-NH_3(1_0 0_0), centred at the frequency of the main hyperfine component (572.4983387 GHz), is shown in Fig. 1 together with the hyperfine structure from Table 3 of Cazzoli et al. (2009), adopting the Local Standard of Rest (LSR) velocity (V_{LSR}) of L1544, 7.2 km s ^{1}, as reported by Tafalla et al. (1998). This is the first observed interstellar o-NH_3(1_0 0_0) spectrum clearly showing the main groups of hyperfine components. The mismatch between the V_{LSR} and the centroid velocity of the main group of hyperfine components is due to heavy self-absorption (from the envelope) combined with Doppler-shifted emission (due to core contraction; Keto & Caselli 2010). In fact, NH_3 is abundant across L1544 (Crapsi et al. 2007), and the outer portions of the contracting pre-stellar core, where the volume density is significantly lower than the critical density of o-NH_3(1_0 0_0), are absorbing the redshifted part of the spectrum that is emitted toward the centre.

Self-absorption and Doppler-shifting due to the dynamics have already been detected in other molecular lines when observed toward the same line of sight. Figure 2 shows a comparison of the only isolated hyperfine component in the spectrum of o-NH_3(1_0 0_0) (F_N^0 ! F_N = 0 ! 1; filled grey histogram) with other lines: $C^{18}O$(1 0), o-H_2D^+(1_{10} 1_{11}), N_2H^+(1 0), HCO^+(1 0), and o-H_2O(1_{10} 1_{01}) (black histograms). The o-NH_3 hyperfine component displays the characteristic blue-shifted infall profile (e.g. Evans 1999), with a self-absorption dip reaching the zero-level, thus indicating a large line optical depth (Myers et al. 1996). It is interesting to note that the NH_3 line shows extra emission at low velocities (coming from the material approaching the core centre from the back) when compared to the low-density tracer $C^{18}O$(1 0), which does not probe the central regions because of the large CO freeze-out

[1] http://archives.esac.esa.int/hda/ui

[2] http://www.iram.fr/IRAMFR/GILDAS

[3] http://herschel.esac.esa.int/twiki/bin/view/Public/HifiCalibrationWeb

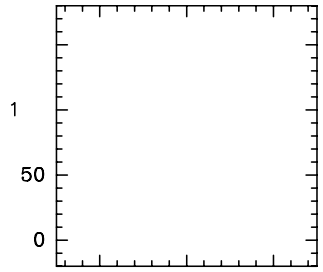

Fig. 2. Comparison between the isolated hyperfine component F_N^0 ! F_N = 0 ! 1 of o-NH_3(1_0 0_0) (filled grey histogram); for clarity, the NH_3 spectrum has been cut above 7.8 km s^{-1} (6.6 km s^{-1} in the velocity scale of Fig. 1), where the other groups of hyperfine components are present and other molecular lines observed toward the same position: $C^{18}O$(1 0), o-H_2D^+(1_{10} 1_{11}), N_2H^+(1 0), HCO^+(1 0), and o-H_2O(1_{10} 1_{01}) (thin histograms). To allow a clearer profile comparison, the $C^{18}O$(1 0), o-H_2D^+(1_{10} 1_{11}), N_2H^+(1 0), and HCO^+(1 0) spectra have been divided by the numbers shown below the transition in the top left corner of the panels. In the case of o-H_2O(1_{10} 1_{01}) (*last panel on the right*), the spectrum has first been multiplied by 4.5 and then shifted by +67 mK. The comparison spectra are in order of increasing optical depth, *from left to right*. The vertical dotted line marks the core velocity.

(Caselli et al. 1999). Extra blue emission of the o-NH_3(1_0 0_0) hyperfine component is also seen when compared to the o-H_2D^+(1_{10} 1_{11}) and N_2H^+(1 0) lines, although to a lesser extent. The "blue excess" disappears in the case of HCO^+(1 0), which is also heavily absorbed (Tafalla et al. 1998). The resemblance between o-NH_3(1_0 0_0) and HCO^+(1 0) is quite striking, in view of the fact that the distribution of HCO^+ across the core is known to be quite different from that of NH_3, with HCO^+ tracing the outer layers of the core while being depleted toward the centre because of the freeze-out of its main parent species CO (Tafalla et al. 2002, 2006). The H_2O line is the most blue-shifted and displays the broadest absorption, thus suggesting higher optical depths (see Keto et al. 2014). This is probably caused by the large abundance of H_2O (compared to NH_3) in the L1544 outer layers, which is responsible for the absorption in a velocity range spanned by the lower density tracers in Fig. 2.

4. Analysis

The non-local thermal equilibrium (non-LTE) radiative transfer code MOLLIE (Keto 1990; Keto et al. 2004; Keto & Rybicki 2010) was used to interpret the o-NH_3(1_0 0_0) spectrum in Fig. 1. We took into account the hyperfine structure, produced by the electric quadrupole coupling of the N nucleus with the electric field of the electrons, as well as the magnetic hyperfine structure that is due to the three protons (Cazzoli et al. 2009). The hyperfine collision rate coefficients were taken from the recent calculations of Bouhafs et al. (2017), which, for the first time, include the non-spherical structure of p-H_2 (the main form of H_2 in cold molecular gas, Flower et al. 2006; Brünken et al. 2014), so that they differ (by up to a factor ' 2) from those of Maret et al. (2009). The calculations were restricted to the lowest nine hyperfine levels of o-NH_3, corresponding to the first two rotational levels (0_0 and 1_0), within a temperature range 5 30 K. Since only the ground-state o-NH_3 transitions were considered, no scaling of the rotational rates was necessary: all hyperfine rates are equal to the pure rotational rates, and intra-multiplet rates are set to zero, as in the standard statistical approach.

Unlike for H_2O and CO (Keto & Caselli 2008; Caselli et al. 2012; Keto et al. 2014), we did not develop any simplified chemistry for NH_3 to be coupled with the hydro-dynamical evolution. Two different approaches were followed to simulate the observed spectrum: (1) the radial profile of o-NH_3 follows that of p-NH_3 deduced by Crapsi et al. (2007) using VLA observations of p-NH_3(1,1), assuming an ortho-to-para NH_3 abundance ratio of 1 and 0.7[4], and extrapolating to larger radii (see Eq. (1)); (2) the radial profile of o-NH_3 was calculated using the chemical model predictions of Sipilä et al. (2015a,b) and Sipilä et al. (2016) applied to the L1544 physical structure deduced by Keto & Caselli (2010) and Keto et al. (2015), who demonstrated that other observed line profiles can be reproduced by the quasi-equilibrium contraction of an unstable Bonnor-Ebert sphere. The two abundance profiles are presented in Fig. 3 together with the profile of H_2O deduced by Caselli et al. (2012) and refined by Keto et al. (2014).

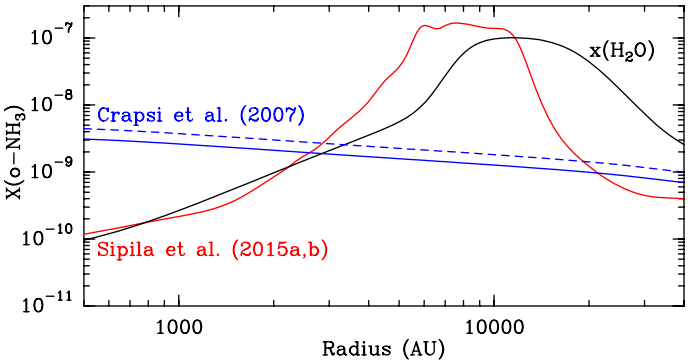

Fig. 3. Radial profile of the fractional abundance of o-NH_3 with respect to H_2, X(o-NH_3), in L1544. The blue profile has been deduced from observations carried out by Crapsi et al. (2007) assuming an ortho-to-para NH_3 abundance ratio of 1 (dashed curve) and 0.7 (solid curve); the red profile is the result of a chemical model calculation by Sipilä et al. (2015a,b). The black profile refers to the total (ortho+para) abundance of H_2O from Keto et al. (2014).

Crapsi et al. (2007) followed the same analysis as Tafalla et al. (2002). They parametrised the abundance profile of total (ortho+para) NH_3, $X_{NH_3}(r)$, starting from X(p-NH_3) and assuming an ortho-to-para ratio of unity, with the function:

$$X_{NH_3}(r) = X_0 \left(\frac{n(r)}{n_0}\right)^{\alpha_X}, \quad (1)$$

[4] Taking into account the calibration errors of the Crapsi et al. (2007) observations, we cannot distinguish between these two values. However, the two slightly different abundance profiles show how possible small variations in the abundance can affect the simulated spectrum.

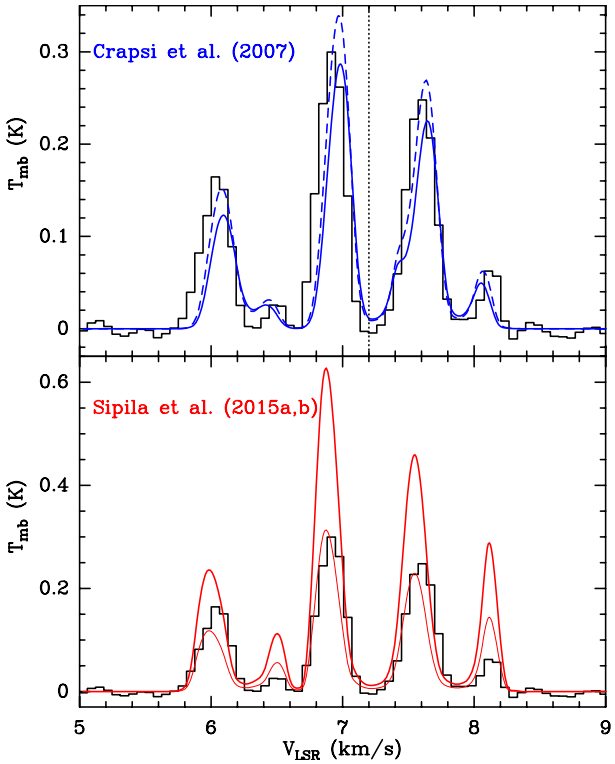

Fig. 4. MOLLIE radiative transfer results using the o-NH_3 fractional abundance profiles from Fig. 3, overlapped with the observed spectrum: (*top*) blue solid and dashed curves refer to the Crapsi et al. (2007) profiles, assuming an ortho-to-para NH_3 ratio of 0.7 and 1.0, respectively. (*Bottom*) The red thick curve refers to the Sipilä et al. (2015a,b) profile; the red thin curve is the same as the thick red curve, but divided by 2.

and then finding the best-fit parameters: X_0 = 8 10 ^{9}, n_0 = 2.1 10^6 cm ^{3} (the average density within a radius of 14^{00}) and α_X = 0.16. The abundance profile of p-NH_3 measured by Crapsi et al. (2007) is given by multiplying the right-hand side of Eq. (1) by 0.5; from this, we derived the abundance profile of o-NH_3 assuming an ortho-to-para NH_3 ratio of 1 (dashed blue curve in Fig. 3) and 0.7 (solid blue curve in Fig. 3). The latter value is expected in cold gas and would indicate a gas-phase formation for NH_3 (Faure et al. 2013). As noted by Tafalla et al. (2002), Crapsi et al. (2007) found that the NH_3 abundance slightly increases toward the core centre. We note that the interferometric observations of Crapsi et al. (2007) have an angular resolution of about 4^{00} (300 AU in radius), so they place stringent constraints on the abundance profile of NH_3[5]. A comparison of the blue curves with the (ortho+para) H_2O abundance profile deduced by Keto et al. (2014) (black curve in Fig. 3) shows that the total NH_3 is about 30 times more abundant than H_2O within the central 1000 AU, while it is two orders of magnitude less abundant than H_2O from about 8000 AU to 20 000 AU.

The o-NH_3 profile has a very different shape when the chemical model of Sipilä et al. (2015a,b), which includes spin-state chemistry, is considered (red curve in Fig. 3). The chemical abundance gradients in L1544 were simulated using the same procedure as described in Sipilä et al. (2016): the physical model for L1544 (Keto & Caselli 2010; Keto et al. 2014) was separated

little toward the centre, when compared with the abundance deduced by the interferometric observations of Crapsi et al. (2007). The predicted large NH_3 abundance at radii around 10 000 AU is mainly caused by surface formation followed by reactive desorption (with 1% efficiency, which may be overestimated). Figure 2 shows that the o-H_2O spectrum is more absorbed around the LSR velocity than that of o-NH_3, suggesting that H_2O is indeed more extended than NH_3 in the outer low-density part of the envelope, while the red curve in Fig. 3 predicts NH_3 abundances around 10 000 AU comparable to those of H_2O (see Fig. 3). Toward the core centre, the predicted low NH_3 abundance indicates that selective desorption mechanisms for NH_3 (e.g. lower binding energies for NH_3 adsorbed on CO and/or N_2 ice layers, formed on top of the water ice, combined with ice heating or disruptive action by cosmic rays; Ivlev et al. 2015), not included in the model, may be at work. Another possibility could be that the production of gas phase NH_3 is underestimated; the N_2 abundance profile drops more slowly than the CO abundance profile in the other pre-stellar core L183 (Pagani et al. 2012), meaning that N_2 desorption is more efficient than currently advocated and/or that production of N_2 is ongoing in the gas phase, thus maintaining efficient production of NH_3 through the usual routes in the gas phase. However, the assumption of a static cloud could also be the cause of the discrepancy with the empirical profile, and this will be discussed in a future paper (Sipilä et al., in prep.). It is clear that more work needs to be done to gain understanding of the gas-grain chemical processes regulating NH_3 and N-bearing molecules in cold and quiescent objects such as L1544, the precursors of future stellar systems.

Acknowledgements. P.C. acknowledges the financial support from the European Research Council (ERC; project PALs 320620). M.T. acknowledges partial support from MINECO project AYA2016-79006-P. C.M.W. acknowledges support from Science Foundation Ireland Grant 13/ERC/I2907. A.F. acknowledges support from the Agence Nationale de la Recherche (ANR-HYDRIDES), contract ANR-12-BS05-0011-01. HIFI has been designed and built by a consortium of institutes and university departments from across Europe, Canada and the United States under the leadership of SRON Netherlands Institute for Space Research, Groningen, The Netherlands and with major contributions from Germany, France and the US. Consortium members are: Canada: CSA, U. Waterloo; France: CESR, LAB, LERMA, IRAM; Germany: KOSMA, MPIfR, MPS; Ireland: NUI Maynooth; Italy: ASI, IFSI-INAF, Osservatorio Astrofisico di Arcetri-INAF; The Netherlands: SRON, TUD; Poland: CAMK, CBK; Spain: Observatorio Astronómico Nacional (IGN), Centro de Astrobiología (CSIC-INTA). Sweden: Chalmers University of Technology – MC2, RSS & GARD; Onsala Space Observatory; Swedish National Space Board, Stockholm University – Stockholm Observatory; Switzerland: ETH Zurich, FHNW; USA: Caltech, JPL, NHSC.

References

Benson, P. J., & Myers, P. C. 1989, ApJS, 71, 89
Bouhafs, N., Rist, C., Daniel, F. et al. 2017, MNRAS, in press DOI: https://doi.org/10.1093/mnras/stx1331
Brünken, S., Sipilä, O., Chambers, E. T., et al. 2014, Nature, 516, 219
Caselli, P., Walmsley, C. M., Tafalla, M., Dore, L., & Myers, P. C. 1999, ApJ, 523, L165
Caselli, P., Walmsley, C. M., Zucconi, A., et al. 2002, ApJ, 565, 331
Caselli, P., Keto, E., Pagani, L., et al. 2010, A&A, 521, L29
Caselli, P., Keto, E., Bergin, E. A., et al. 2012, ApJ, 759, L37
Cazzoli, G., Dore, L., & Puzzarini, C. 2009, A&A, 507, 1707
Ceccarelli, C., Baluteau, J.-P., Walmsley, M., et al. 2002, A&A, 383, 603
Cheung, A. C., Rank, D. M., Townes, C. H., Thornton, D. D., & Welch, W. J. 1968, Phys. Rev. Lett., 21, 1701
Codella, C., Lefloch, B., Ceccarelli, C., et al. 2010, A&A, 518, L112
Crapsi, A., Caselli, P., Walmsley, M. C., & Tafalla, M. 2007, A&A, 470, 221
Danby, G., Flower, D. R., Valiron, P., Schilke, P., & Walmsley, C. M. 1988, MNRAS, 235, 229
de Graauw, T., Helmich, F. P., Phillips, T. G., et al. 2010, A&A, 518, L6
Evans, II, N. J. 1999, ARA&A, 37, 311
Faure, A., Hily-Blant, P., Le Gal, R., Rist, C., & Pineau des Forêts, G. 2013, ApJ, 770, L2
Flower, D. R., Pineau Des Forêts, G., & Walmsley, C. M. 2006, A&A, 449, 621
Gerin, M., Neufeld, D. A., & Goicoechea, J. R. 2016, ARA&A, 54, 181
Hjalmarson, Å., Bergman, P., Biver, N., et al. 2005, Adv. Space Res., 36, 1031
Ho, P. T. P., & Townes, C. H. 1983, ARA&A, 21, 239
Ivlev, A. V., Röcker, T. B., Vasyunin, A., & Caselli, P. 2015, ApJ, 805, 59
Keene, J., Blake, G. A., & Phillips, T. G. 1983, ApJ, 271, L27
Keto, E. R. 1990, ApJ, 355, 190
Keto, E., & Caselli, P. 2008, ApJ, 683, 238
Keto, E., & Caselli, P. 2010, MNRAS, 402, 1625
Keto, E., & Rybicki, G. 2010, ApJ, 716, 1315
Keto, E., Rybicki, G. B., Bergin, E. A., & Plume, R. 2004, ApJ, 613, 355
Keto, E., Rawlings, J., & Caselli, P. 2014, MNRAS, 440, 2616
Keto, E., Caselli, P., & Rawlings, J. 2015, MNRAS, 446, 3731
Larsson, B., Liseau, R., Bergman, P., et al. 2003, A&A, 402, L69
Lis, D. C., Wootten, H. A., Gerin, M., et al. 2016, ApJ, 827, 133
Liseau, R., Larsson, B., Brandeker, A., et al. 2003, A&A, 402, L73
Maret, S., Faure, A., Scifoni, E., & Wiesenfeld, L. 2009, MNRAS, 399, 425
Myers, P. C., Mardones, D., Tafalla, M., Williams, J. P., & Wilner, D. J. 1996, ApJ, 465, L133
Ott, S. 2010, in Astronomical Data Analysis Software and Systems XIX, eds. Y. Mizumoto, K.-I. Morita, & M. Ohishi, ASP Conf. Ser., 434, 139
Pagani, L., Bourgoin, A., & Lique, F. 2012, A&A, 548, L4
Persson, C. M., Olofsson, A. O. H., Koning, N., et al. 2007, A&A, 476, 807
Persson, C. M., Olberg, M., Hjalmarson, Å., et al. 2009, A&A, 494, 637
Persson, C. M., Black, J. H., Cernicharo, J., et al. 2010, A&A, 521, L45
Pillai, T., Wyrowski, F., Carey, S. J., & Menten, K. M. 2006, A&A, 450, 569
Salinas, V. N., Hogerheijde, M. R., Bergin, E. A., et al. 2016, A&A, 591, A122
Sipilä, O., Caselli, P., & Harju, J. 2015a, A&A, 578, A55
Sipilä, O., Harju, J., Caselli, P., & Schlemmer, S. 2015b, A&A, 581, A122
Sipilä, O., Spezzano, S., & Caselli, P. 2016, A&A, 591, L1
Tafalla, M., & Bachiller, R. 1995, ApJ, 443, L37
Tafalla, M., Mardones, D., Myers, P. C., et al. 1998, ApJ, 504, 900
Tafalla, M., Myers, P. C., Caselli, P., Walmsley, C. M., & Comito, C. 2002, ApJ, 569, 815
Tafalla, M., Santiago-García, J., Myers, P. C., et al. 2006, A&A, 455, 577
van Dishoeck, E. F., Kristensen, L. E., Benz, A. O., et al. 2011, PASP, 123, 138
Wyrowski, F., Güsten, R., Menten, K. M., Wiesemeyer, H., & Klein, B. 2012, A&A, 542, L15
Wyrowski, F., Güsten, R., Menten, K. M., et al. 2016, A&A, 585, A149